An Electrically Engineered Meta-Material Absorber

Shi (Mark) Gu

Advised By: Dr. Steven Cummer

Submitted in Partial Fulfillment of Graduation with Distinction Requirements On:

4-20-2009

Abstract

Recent developments in artificially engineered metamaterials have enabled the creation of electromagnetic materials with properties not found in nature. Much work has centered on designing split ring resonators (SRR's) and electrical coupled LC resonators (ELC's) to create bulk mediums with desired effective permittivity and permeability. Recent work has demonstrated the feasibility of developing electromagnetic absorbers using such metamaterials. This thesis builds on that work and presents the design, simulation, and experimental verification of a broadband GHz region metamaterial absorber, with a max absorption of 94% at 2.7 GHz, with a half-max bandwidth of .217 GHz.

Table of Contents

I. Introduction

The artificial properties of electrically engineered metamaterials were first theorized by Vesalago[1], who showed the theoretical possibility of materials with simultaneously negative permittivity, ε, and permeability, μ. Recent research in metamaterials have let to practical implementations of such materials. One of the earliest approaches utilizes split ring resonators (SRR's) to generate a Lorentzian-shaped resonant magnetic response[2], along with thin-wires to generate a broadband electrical response. Alternating layers of these SRR's and thin wires, as long as they are much smaller than wavelength (<< λ/5) will produce a simultaneously negative ε_r and μ_r[3]. Subsequent experiments using a two-dimensional array of copper strips and SRR's experimentally verified the negative refraction properties of such metamaterials[4].

Another method of generating an electrical response is with an electrically coupled LC resonator (ELC)[5]. Unlike thin wires, ELC's are resonant structures that exhibit a Lorentzian response similar to that of the SRR, except in permittivity instead of in permeability. Alternating layers of tuned SRR's and ELC's have been shown to result in simultaneously negative ε_r and μ_r, resulting in negative refraction[6]. Utilizing variations of these three basic structures, SRR's, ELC's, and thin wires, absorption of electromagnetic energy can be achieved either through resistive or dielectric loss. Landy, et al demonstrated a near perfect narrowband absorber in the THz region by using an electric-SRR, copper strip, and dielectric based metamaterial[7]. It was shown that most of the loss was due to dielectric loss, which is generally the primary source of loss for most resonant metamaterials[8]. Subsequent work by Tao, et al replaced the copper strip with a complete backplane, and was able to achieve 96% absorption at 1.6 THz, with a 16μm thick surface, and with good broad angle performance for both TE and TM modes[9].

II. Design and Simulation

In this paper, I present the design, simulation, and experimental testing of a GHz region metamaterial absorber that uses a combination of ELC's and SRR's to achieve 94% absorption at 2.7GHz with a half-max bandwidth of .217GHz. The design of this absorber differs from previous work in its use of lumped resistive elements as the chief contributor of absorption. Furthermore, this absorber is designed to be a perfectly matched layer i.e. n=1, both in and out of resonance. This differs from the metamaterial designs used in Landy, *et al.* and Tao, *et al.* which were perfectly matched at resonance but had high reflection out of band. Thus, this metamaterial design is an absorber/transmitter rather than an absorber/reflector. The use of resistors and a backplane-less metamaterial design was mentioned by Bilotti[10], but was not experimentally tested and did not utilize the concept of using a PML to decrease reflection.

The theoretical basis for this design comes from the relationships between the relative permittivity, relative permeability, index of refraction, and impedance i.e. ε_r, μ_r, n, and z of the SRR and ELC particles. For both particles, as long as they are electrically small, these bulk parameters hold and are related by the following equations:

$$z = \sqrt{\frac{\mu_r}{\varepsilon_r}} \qquad \textbf{Equation 1}$$

$$n = \sqrt{\mu_r \varepsilon_r} = \sqrt{(\varepsilon'\mu' - \varepsilon''\mu'') + j(\mu''\varepsilon' + \varepsilon''\mu')} = \sqrt{x + jy} \qquad \textbf{Equation 2}$$

$$n = \sqrt{x + jy} = \sqrt{\frac{r+x}{2}} + \frac{jy}{\sqrt{2(r+x)}} \qquad r = \sqrt{x^2 + y^2} \qquad \textbf{Equation 3}$$

where $n < 0$ when $\mu_r < 0$ and $\varepsilon_r < 0$. Furthermore, the incident electromagnetic field is attenuated inside the effective medium of the particle by Im(n) as show below. Let's use a wave propagating in the **x** direction with electric field polarized in the +**y** direction as an example (time dependence is assumed here):

$$E(x) = \mathbf{y}E_o e^{-j\beta x} \qquad \textbf{Equation 4}$$

$$E(x) = \mathbf{y}E_o e^{-j\beta x} = \mathbf{y}E_o e^{-j\omega\sqrt{\varepsilon_0\mu_0}\sqrt{\varepsilon\mu}x} = \mathbf{y}E_o e^{-j\omega\sqrt{\varepsilon_0\mu_0}\,\mathrm{Re}(n)x} e^{-j\omega\sqrt{\varepsilon_0\mu_0}\,(j\,\mathrm{Im}(n))x} \qquad \textbf{Equation 5}$$

Where $$\mathrm{Im}(n) = \frac{(y)}{\sqrt{2(r+y)}} \qquad \textbf{Equation}$$

If $y = \mu_r''\varepsilon_r' + \varepsilon_r''\mu_r'$ is negative, then the electromagnetic wave is decaying with **x,** indicating loss. Note that, in general, a electromagnetic wave propagating through a passive medium will have $\mu_r'' < 0$ and $\varepsilon_r'' < 0$. Thus, there will be loss as long as $\mu_r' > 0$ and $\varepsilon_r' > 0$. This relationship indicates that the more negative Im(n) is, the more loss is generated. Intuitively, larger magnitudes of ε_r and μ_r will result in larger fields in the material. The energy from these fields can be lost through resistive and dielectric heating, which can be increased or decreased by varying the resistance. In practice, loss is measured by the amount of electromagnetic power absorbed, where absorbed power, *A,* is related to the reflected power, *R*, the transmitted power, *T*, and the reflection coefficient S_{11} and transmission coefficient S_{21} by:

$$A = 1 - R - T \text{ and } A = 1 - S_{11}^{\ 2} - S_{21}^{\ 2} \qquad \textbf{Equation 7}$$

Furthermore, since the SRR and ELC particles are essentially RLC resonators[2], one can change the resonant frequency, $\omega_o = \frac{1}{\sqrt{LC}}$ and Q value, $Q = \frac{1}{R}\sqrt{\frac{L}{C}}$, by changing R, L, and C for a given metamaterial particle. L and C values were adjusted in order to tune the strong, Lorentzian magnetic response of the SRR such that it overlays the strong Lorentzian electric response of the ELC to create a lossy, yet perfectly matched effective medium. Once this is accomplished, R can be adjusted to achieve the desired Q-value, where an increase in R yields a flatter, lower Q response, and a decrease in R yields a sharper, higher Q response.

Figure 1 shows one unit-cell of an ELC particle, with its simulated reflection and transmission response using Ansoft HFSS shown in Figure 2.

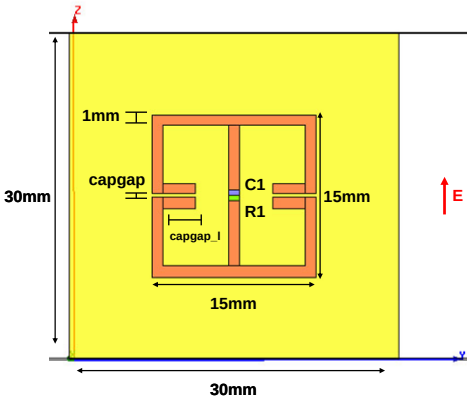

Figure 1: ELC

Please note that all variable parameter values for the particles shown in all figures can be found in Appendix A. In Figure 2, the S_{21} minima and S_{11} maxima indicate a resonant frequency of 2.6GHz. The absorbed, reflected, and transmitted power of this ELC is shown in Figure 3, with a maximum absorption of 47%. The half-max absorbed power bandwidth is found to be .26 GHz. By varying the lumped resistor on the ELC, maximum absorption can be traded off with bandwidth until a desired balance between the two is achieved. Similarly,

varying the *capgap* of the ELC can change its total capacitance, and therefore shift the resonant frequency. It's important to note that the capacitance of the two gaps are each on the order of 1pF, whereas the lumped capacitors used in the ELC typically had values of 2 to 10pF. It was theorized that these three capacitances are in series with an equivalent capacitance shown in Equation 8.

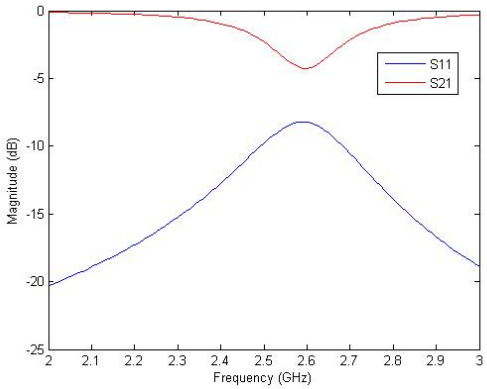

Figure 2: Simulated ELC S11 and S21

$$\frac{1}{C_{eq}} = \frac{1}{C_1} + \frac{1}{C_2} + \ldots + \frac{1}{C_n} \qquad \textbf{Equation 8}$$

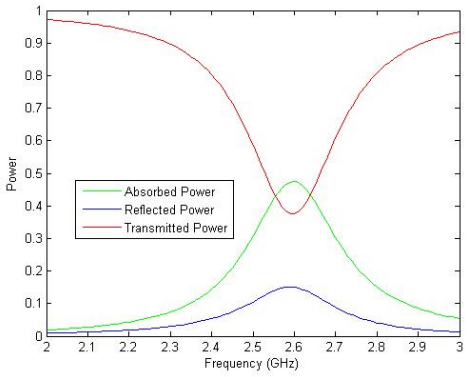

Figure 3: Simulated ELC Power

Thus, variations in the value of the larger lumped capacitor do not change the resonant frequency significantly, and varying the *capgap* was the primary method by which the resonant frequency was tuned.

Once the desired response was achieved, a Matlab parameter retrieval based on Smith, *et al* [11] [12] and developed by Popa[13] was used in order to extract ε_r, μ_r, n, and z from the simulated S_{11} and S_{21} responses. The retrieval technique assumed TEM incidence and was based on the three slab configuration shown in Figure 4.

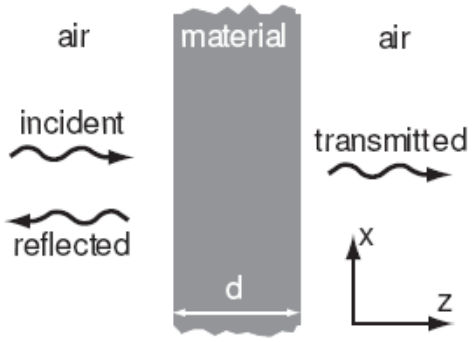

Figure 4: Three Slab Configuration

The reflection and transmission coeffecients at the material interfaces are found to be:

$$T = \frac{(1-\Gamma^2)e^{-2jk_0nd}}{1-\Gamma^2 e^{-2jk_0nd}}$$

$$R = \Gamma\frac{1-e^{-2jk_0nd}}{1-\Gamma^2 e^{-2jk_0nd}}$$

Equation 9

Where d is the thickness of the material, k_0 is the wavenumber in free space, and Γ is the local reflection coefficient:

$$\Gamma = \frac{z-1}{z+1}$$

Equation 10

Inverting the equations gives:

$$z = \pm\sqrt{\frac{(1+R)^2 - T^2}{(1-R)^2 - T^2}}$$

$$n = \pm\frac{1}{k_0 d}\left[\cos^{-1}\left(\frac{1-R^2+T^2}{2T}\right) + 2\pi m\right]$$

Equation 11

Where m is an arbitrary integer. From n and z, the effective material parameters can be derived as:

$$\varepsilon_y = \varepsilon_0 \frac{n}{z}$$

$$\mu_x = \mu_0 n z$$

Equation 12

As mentioned by Bogdan, there is some ambiguity in choosing the branch number m, when performing the retrieval. However, it is not too difficult as

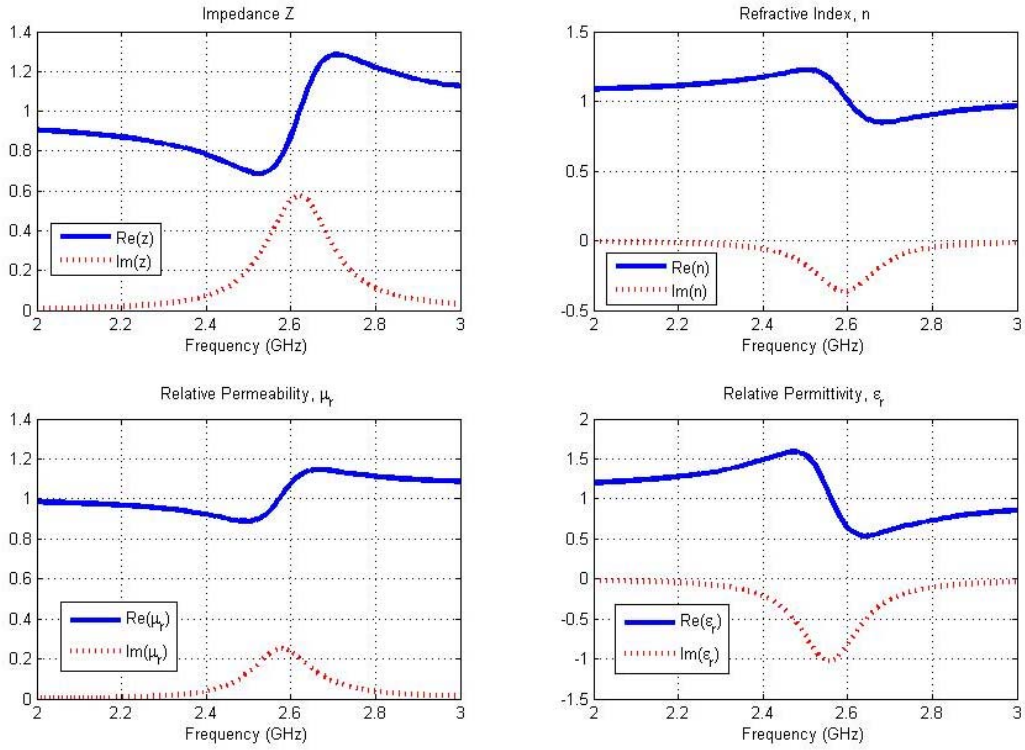

Figure 5: ELC Retrieved Parameters

long as the thickness of the unit cell, *d*, is much smaller than wavelength. Furthermore, one needs to be careful to place the simulated wave ports at least λ/2 from the particle interface itself in order to avoid any near-field coupling. This in turn means that one needs to de-embed the simulated S11 and S21 results before using the retrieval technique in order to get the proper phase response of the particle.

Figure 5 shows the parameter retrieval performed on the aforementioned simulated ELC particle. Note the Lorentzian response in ε_r, with a maxima of 1.6 and a minima of .5. Note that it's centered at around 1.2 when not at resonance. This non-unity ε_r is due to the fact that the FR4 dielectric, which has ε_r=4, dominates out of resonance. Note also that μ_r is close to one outside of resonance, but has a small anti-resonance at the resonant frequency. This anti-resonance is generally too small to have much practical significance. Since *z* and *n* are related to ε_r and μ_r, they also take on non-unity values at resonance. Note that a non-unity *z* at resonance means greater reflection since the effective medium is not matched to air. Similarly, a non-unity *n* means that the effective index of refraction of the medium is different than that of air. Finally, a look at the imaginary part of *n* indicates that there is loss, or absorbed power, at resonance since Im(*n*) is negative at resonance.

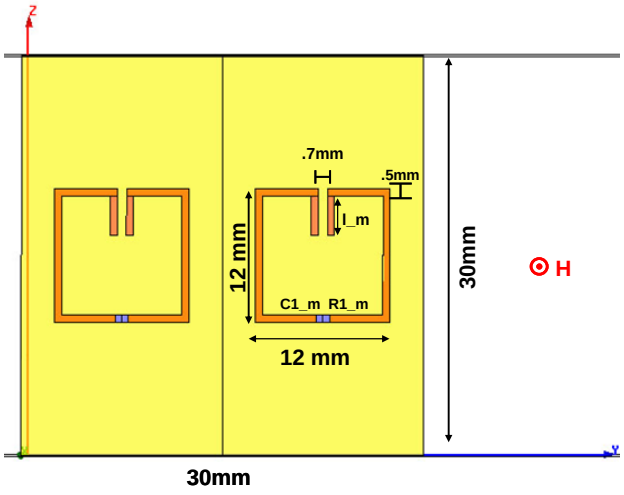

Figure 6: SRR

A similar process of design and simulation was performed for the SRR. Figure 6 shows one unit-cell of an SRR particle. Once again, the lumped resistance and capacitive gap dimensions were varied until a desired maximum absorption and bandwidth was achieved. The final simulated reflection and

transmission response using Ansoft HFSS is shown in Figure 7. Note that the S_{21} minima and S_{11} maxima indicate the resonant frequency of 2.63GHz. The absorbed, reflected, and transmitted power of this SRR is shown in Figure 8, with a maximum absorption of 40%. The half-max absorbed power bandwidth is found to be .15 GHz.

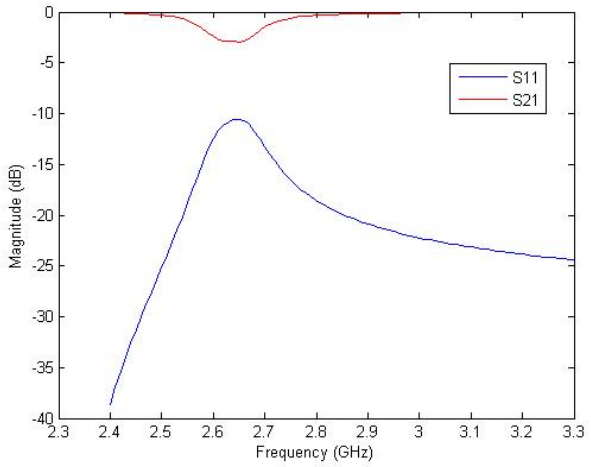

Figure 7: SRR Simulated Response

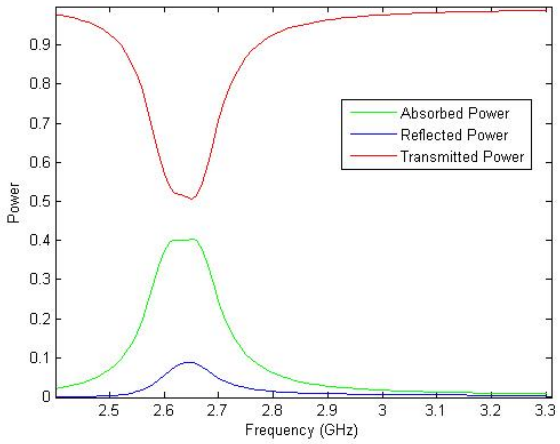

Figure 8: SRR Power

Once again, a parameter retrieval was performed and the results are shown in Figure 9. The SRR effective parameters are quite similar, qualitatively, to the ELC effective parameters except that the Lorentzian resonance is in μ_r instead of ε_r. As mentioned earlier, this mirror-image response is one of the key motivations for this ELC-SRR absorber. By combining the ELC parameter response with the SRR parameter response, one can achieve Lorentzian resonances in both ε_r and μ_r of similar magnitude and bandwidth. The impedance, z, would then been close to unity while n, and more importantly, Im(n) will be large and broad.

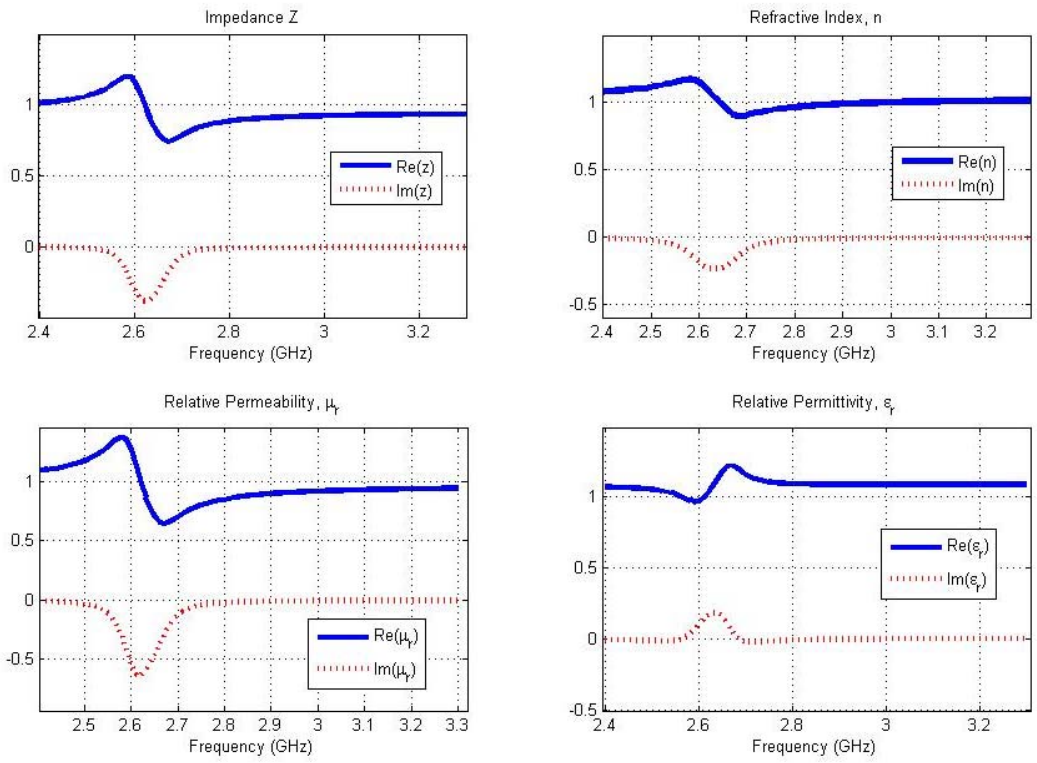

Figure 9: SRR Retrieved Parameters

An ELC-SRR was thus designed and simulated. Several arrangements were simulated, with the constraints that the ELC-SRR had to be much smaller than the wavelength, and that the ELC's and SRR's were arranged in such a way as to fit as many of them in per unit-volume, to maximize absorption per unit volume, while reducing cross-coupling between the constituent particles as much as possible.

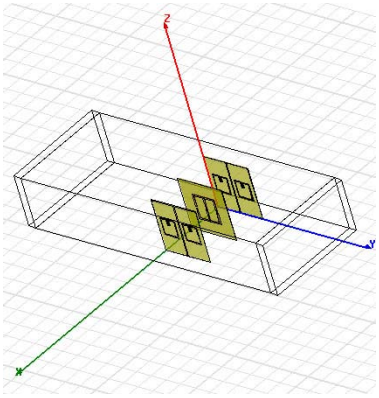

Figure 10: ELC-SRR

The final design that optimized these benchmarks is shown in Figure 10. Its simulated response is shown in Figure 11, and the power response is shown in Figure 12. 95% absorption was achieved at 2.65 GHz, with a half-max

power bandwidth of .3 GHz. Furthermore, the reflected power is below 5% throughout the range, indicating a well-matched effective medium. The dotted lines in Figure 12 show the ELC response in comparison, which has significantly less absorption and more reflection. The parameter retrievals, shown in Figure 13 indicate that this high-absorption, low-reflection performance is due to the aforementioned similarity between the ε_r and μ_r responses. These simulations were thus consistent with theory, and provided a basis for experimental testing.

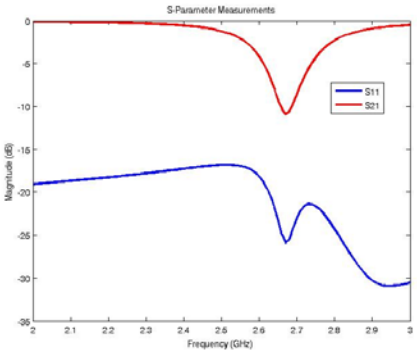

Figure 11: ELC-SRR Simulated Response

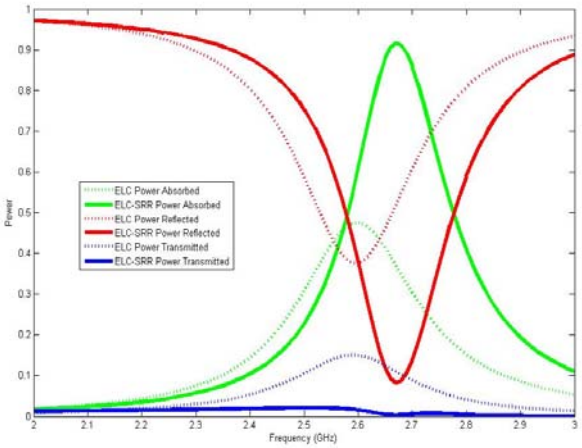

Figure 11: ELC-SRR Power

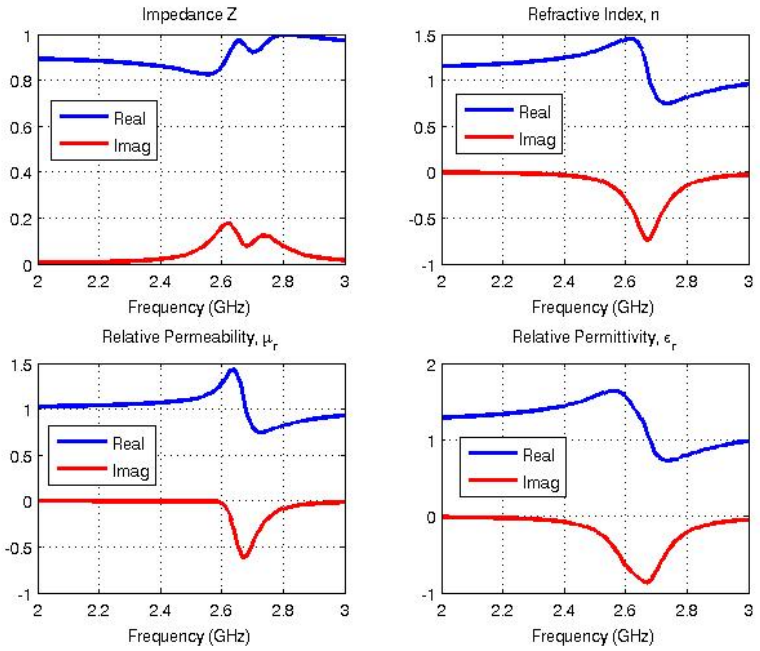

Figure 13: ELC-SRR Retrieved Parameters

III. Experimental Testing

The ELC's and SRR's were fabricated separately using optical mask lithography on FR4 dielectric. Once fabricated, the lumped resistors and capacitors were soldered on. One unit cell of the absorber structure was mounted on a foam support and measurements were taken on a WR340 closed waveguide between 2-3 GHz, as shown in Figure 14. At these frequencies, propagation is confined to the TE_{10} mode. S_{11} and S_{21} measurements were made for one unit-cell of the ELC-SRR absorber as well as for just the constituent ELC and SRR particles. Figure 15 shows that the ELC-SRR has the deepest and broadest

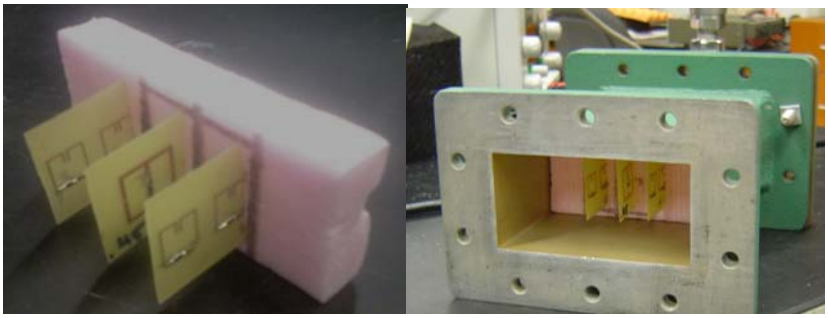

Figure 14: ELC-SRR Absorber

transmission minima, and moreover, has the lowest reflection. This result is strong evidence that the ELC-SRR is able to achieve greater absorption with minimal reflection at resonance by being simultaneously well-matched and lossy. Figure 15 shows the calculated absorbed power, and the ELC-SRR is able to achieve 86% absorption at 2.74GHz with a 50% power bandwidth of .17 GHz.

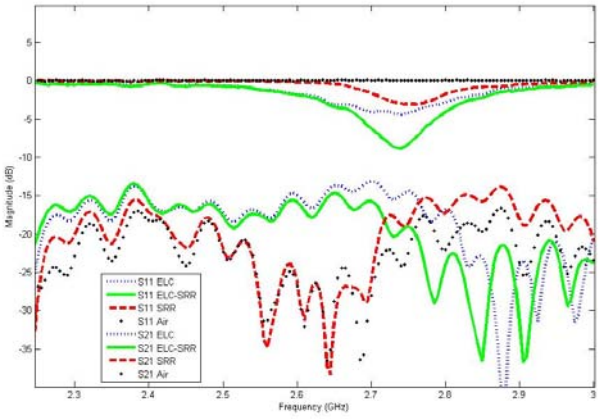

Figure 15: ELC-SRR Absorber Response

After verifying that the ELC-SRR worked as expected, additional work was performed to maximize the absorption and bandwidth of the ELC-SRR. There are two general approaches to increasing maximum absorption and bandwidth. Each of them was tried, with some success, and the results are described below.

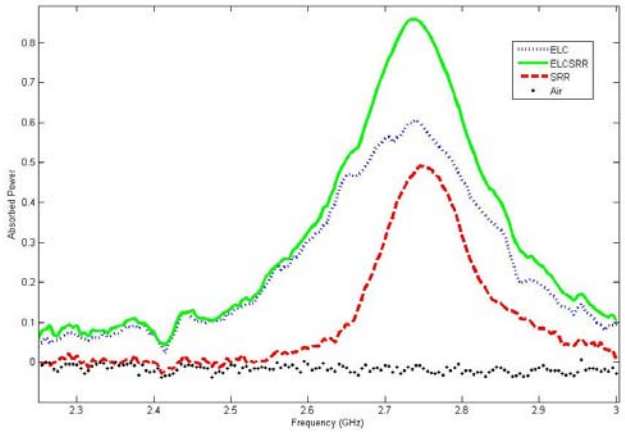

Figure 16: ELC-SRR Absorber Power

1. **Increasing the number of particles per unit cell to increase the peak absorption and bandwidth.**

This approach is relatively straightforward and produced the best experimental results. Two ELC-SRR's, one with one ELC and four 5 Ω SRR's, and the other with one ELC and six 10Ω SRR's were tested. Their S11, S21, and Power measurements are shown in Figures 16 and 17. Maximum absorption of 98.75% is achieved for the ELC-SRR with 5Ω resistors on the SRR's, while a greater bandwidth of .217 GHz is achieved using 10Ω resistors on the SRR's. This latter configuration, with 94% max absorption at 2.7 GHz and .217 GHz half-max bandwidth is the best broadband absorber shown in this thesis.

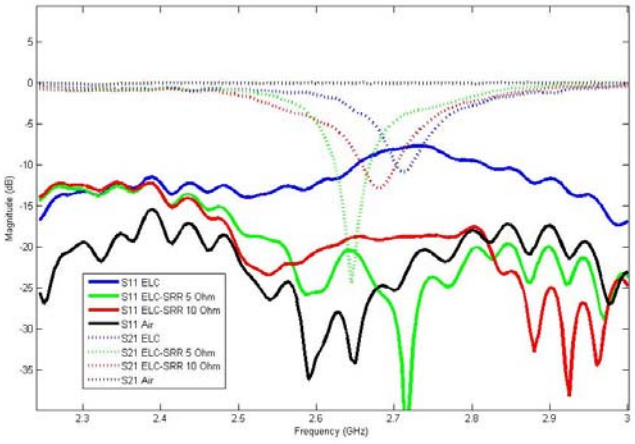

Figure 17: ELC-SRR Response with Multiple SRR's

The limiting factor at the time of writing this thesis is the number of particles that can be packed into one unit cell. As the particles are packed closer and closer

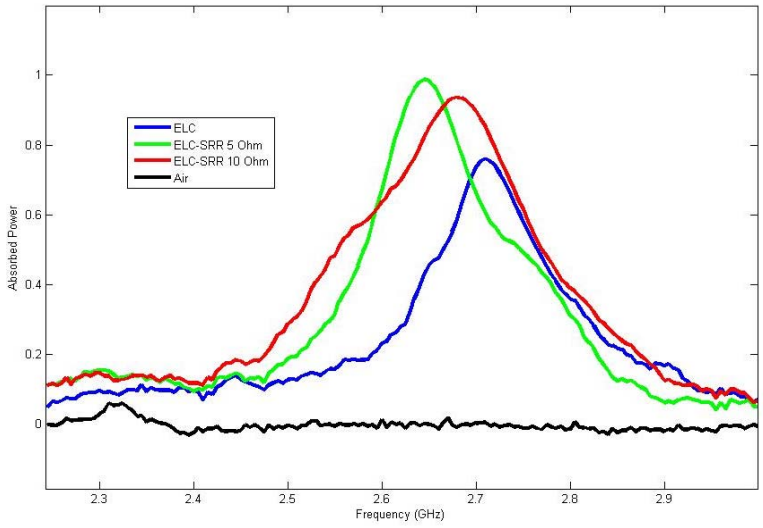

Figure 18: ELC-SRR Power with Multiple SRR's

together, as shown in Figure 23, cross-coupling occurs. This is especially pertinent for the SRR's, due to increased mutual inductance.
The resonant frequency shifts lower as the particles are packed closer together, causing the ELC and SRR resonances to no longer be aligned, therefore making the ELC-SRR imperfectly matched. Further experimental data and discussion of this issue is presented in section IV.

2. **Increasing the number of particles per unit cell, and then using multiple ELC-SRR combinations with different resonances in one unit cell in order to cover a larger bandwidth.**

This approach was also successful in increasing the bandwidth. A unit cell containing 2 ELC's and 7 SRR's, with half of the ELC's and SRR's resonant at one frequency and the other half at a slightly lower frequency was created. It was compared with a unit cell of ELC's and SRR's having the same resonance. The results are shown in Figures 19 and 20. In Figure 20, it is easy to see that the ELC-SRR with a single resonance has a higher max absorption of 98%, with a .2 GHz

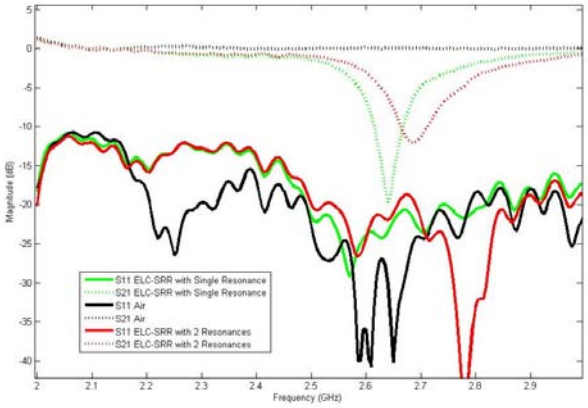

Figure 19: ELC-SRR Response with Multiple Resonances

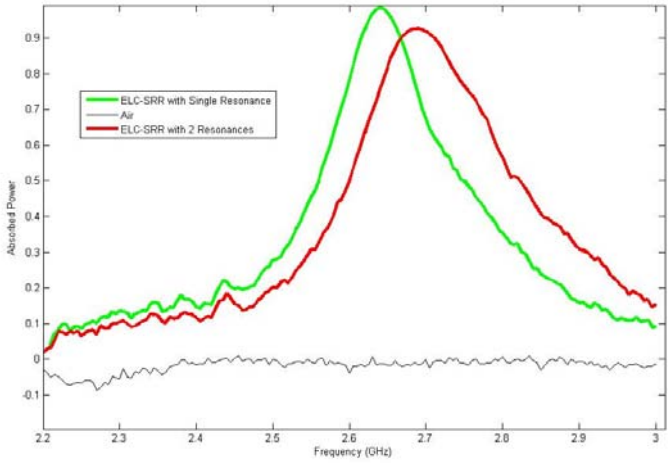

Figure 20: ELC-SRR Power with Multiple Resonances

bandwidth. The double-resonance ELC-SRR has a broader bandwidth of .22 GHz, but a lower max absorption of 92.5%.

IV. Future Work

As mentioned in section III, the primary limitation of the current ELC-SRR design is that as more particles are packed into a unit cell, the particles begin to interact more heavily, and their effective parameters may change. The SRR's, in particular, have increased mutual inductance, and thus their resonant frequency will shift down. The key is that the resonant frequency of the corresponding ELC does not shift down along with the SRR's since the ELC is primarily excited by the electric field and does not couple as strongly with the SRR's. Therefore, one must figure out the resonance of the SRR's when they are packed together, and then design an ELC that is resonant at that frequency. Figure 21 shows such a closely-packed ELC-SRR sandwich using thin foam spacers, with 1 ELC and 10 SRR's.

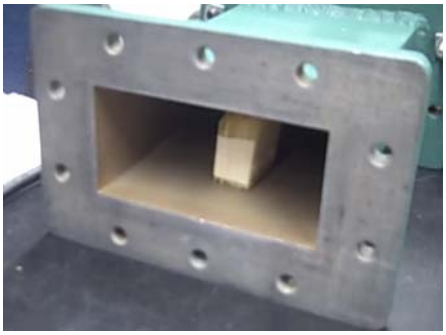

Figure 21: ELC-SRR Sandwich

The response of the SRR's by themselves, the ELC, and the ELC-SRR is shown in Figures 22 and 23. The first thing to note in Figure 22 is that the SRR resonance is shifted down to ~2.2GHz, from

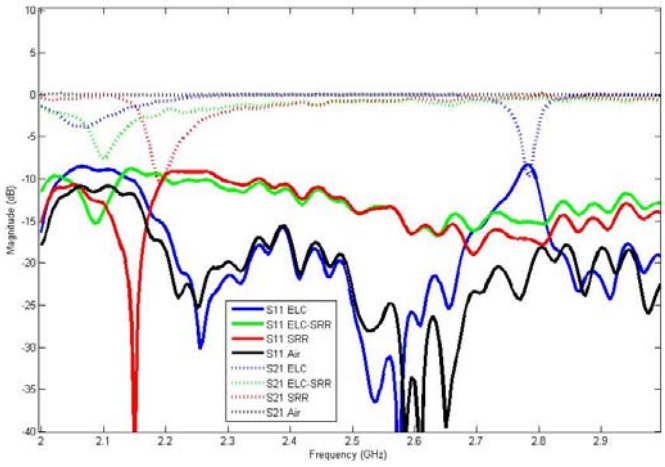

Figure 22: ELC-SRR Sandwich Response

~2.65 GHz for a single particle. The ELC was designed to resonant at ~2.1GHz, although there is a second order resonance at 2.8GHz. At the 2.1 GHz resonance, the ELC exhibits a transmission minima and a reflection maxima. When the SRR's are added, the ELC-SRR now has a simultaneous transmission minima and reflection minima, which indicates absorption, as shown in Figure 22. The absorption peaks in Figure 23 show that increasing the number of SRR's does increase the magnitude of the response compared to previous designs in section III. However, the ELC-SRR combination is not as well matched as those in section III, and therefore there is significant reflection, and relatively narrow bandwidth. These figures thus illuminate the experimental feasibility of packing ELC's and SRR's tightly together to increase the response, but also suggest that more careful resonance matching needs to be done before the full benefits are realized.

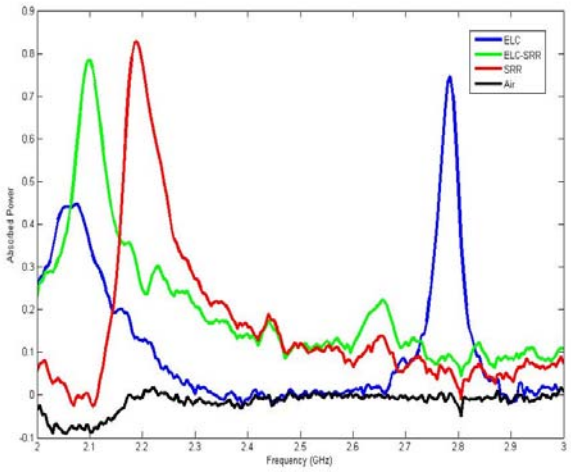

Figure 23: ELC-SRR Power

The ability to tightly pack ELC's and SRR's can also be used to dramatically increase the bandwidth by packing ELC's and SRR's of different resonances together into one unit cell, as mentioned in section III. Preliminary design work has been completed that demonstrate a wide range of ELC's and SRR's with different resonances that span the 2-3 GHz range. The responses of these particulars are shown in Figure 24, 25, and 26, including both simulated and experimental values. Please note that Figure 26 contains experimental measurements of single SRR particles. These resonances will shift down to cover the 2-3 GHz range when they are packed together. Future work will involve careful selection

and spacing of ELC's and SRR's with different resonances in order to achieve 90%+ absorption across the 2-3 GHz range.

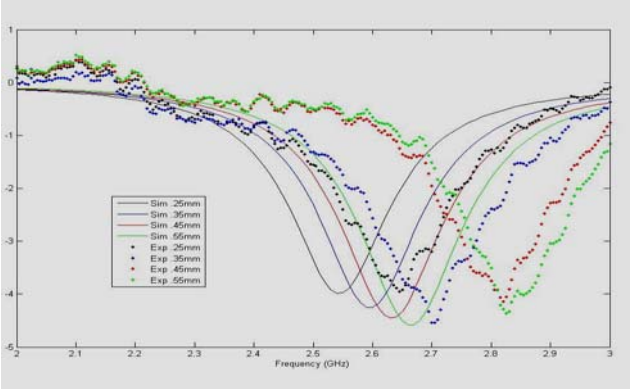

Figure 24: ELC Responses

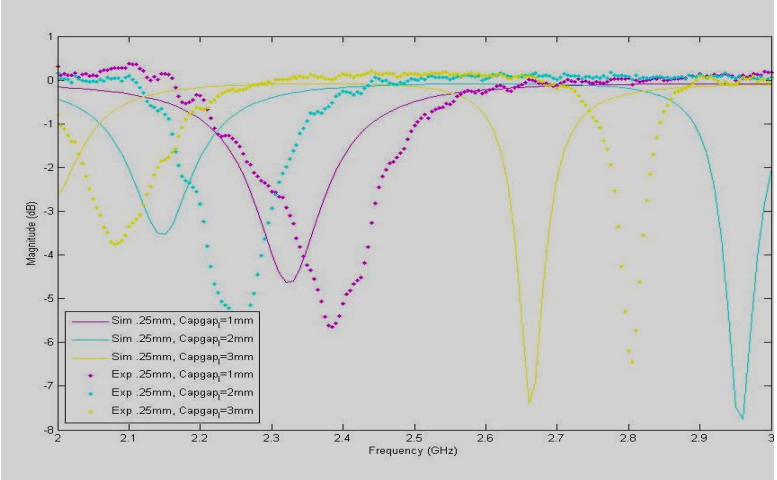

Figure 25: ELC Simulated and Experimental Responses

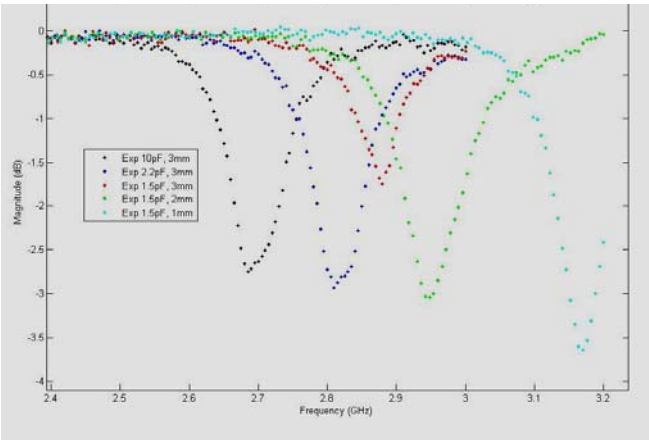

Figure 26: SRR Experimental Responses

V. Conclusion

The work presented in this thesis has demonstrated that a broadband ELC-SRR absorber can be created by precisely overlapping the permittivity and permeability of its constituent ELC's and SRR's in order to create a lossy, yet perfectly matched effective medium. Furthermore, the performance of the absorber can be adjusted by varying its capacitance and/or by adjusting the lumped resistances. By doing so, an ELC-SRR absorber with 94% max absorption at 2.7GHz, and .217 GHz half-max bandwidth was achieved. It was also shown that using an ELC-SRR absorber with multiple resonances can lead to increased bandwidth. Finally, the ground work was laid for future work involving densely packed ELC-SRR absorbers in order to achieve high absorption across the 2-3 GHz frequency band.

VI. Acknowledgements

This thesis would not have been possible without the tremendous support that I received from my colleagues in Dr. Steven Cummer's lab, as well as from my friends and family. I thank Dr. Steven Cummer for letting me into his lab as an undergraduate, and for his insightful guidance throughout the last year. Once I began my work, perhaps no one was more helpful than Dr. Thomas Hand, who went out of his way on a daily basis to teach me even while busily completing his own Ph.D. work. I also thank Dr. Bogdan Popa for his help in the lab, and John Barrett for getting me interested in the first place. Sani Hadziahmetovic and Doug Bycoff, who just recently joined, have also been a lot of fun to work with. Finally, I would like to thank my parents, Yian Gu and Ying Zhou, my twin brother Tim Gu, as well as my friend Rui Dong for their support throughout this whole time.

VII. References

[1] V. G. Veselago. The electrodynamics of substances with simultaneously negative values of ε and μ . *Soviet Physics USPEKI*, 10:509{514, 1968.

[2] J. Pendry, A. Holden, D. Robbins, and W. Stewart. Magnetism from conductors and enhanced nonlinear phenomena. *IEEE Trans. on Microwave Theory and Tech.*, 47:2075, 1999.

[3] D.R. Smith, W. J. Padilla, D. C. Vier, S. C. Nemat-Nasser, S. Schultz. Composite Medium with Simultaneously Negative Permeability and Permittivity. *Phys. Rev. Letters.* **84,** 4184 (2000)

[4] R.A. Shelby, D.R. Smith, S. Schultz. Experimental Verification of a Negative Index of Refraction. *Science* **292,** 77 (2001)

[5] D. Schurig, J. J. Mock, and D. R. Smith. Electric-field-coupled resonators for negative permittivity metamaterials. *Applied Physics Letters*, 88:041109, 2006b.

[6] R. Liu, J.J. Mock, D.R. Smith. Negative index materials composed of electric and magnetic resonators. *Applied Physics Letters* 90, 263504 (2007)

[7] N.I. Landy, S. Sajuyigbe, J.J. Mock, D.R. Smith, and W.J. Padilla. Perfect Metamaterial Absorber, *Physical Review Letters* **100,** 207402 (2008)

[8] T. Hand. Ph.D. Diss., Duke University (2009)

[9] Hu Tao, C. M. Bingham, A. C. Strikwerda, D. Pilon, D. Shrekenhamer, N. I. Landy, K. Fan, X. Zhang, W. J. Padilla, and R. D. Averitt. Highly flexible wide angle of incidence terahertz metamaterial absorber : Design, fabrication, and characterization. *Physical Review B* **78,** 241103(R) (2008)

[10] F. Biloti, L. Nucci, L. Vegni, An SRR based microwave absorber. *Microwave and Optical Technology Letters*. Vol. 48 Issue 11, pp. 2171-2175

[11] D. R. Smith, S. Schultz, P. Markos, and C. M. Soukoulis. Determination of effective permittivity and permeability of metamaterials from reflection and transmission coefficients. *Physical Review B*, 65(195104), 2002.

[12] D. R. Smith, J. J. Mock, A. F. Starr, and D. Schurig. Gradient index metamaterials. *Physical Review E*, 71:036609, 2005a.

[13] B.-I. Popa. "Simplified Design Techniques for Physically Realizable Metamaterials and Applications", Ph.D Diss., Duke University (2007)

Appendix A

Figure	Particle (ELC/SRR)	Quantity	ELC Properties					SRR Properties		
			Capgap (mm)	Capgap_l (mm)	C1(pF)	R1(Ω)		l_m (mm)	C1_m (pF)	R1_m (Ω
1	ELC	1	0.35	0	10	10				
2	ELC	1	0.35	0	10	10				
3	ELC	1	0.35	0	10	10				
5	ELC	1	0.35	0	10	10				
6	SRR	1						3	10	5
7	SRR	1						3	10	5
8	SRR	1						3	10	5
9	SRR	1						3	10	5
10	ELC	1	0.3	0	2.67	10				
10	SRR	2						3	10	10
11	ELC	1	0.3	0	2.67	10				
11	SRR	2						3	10	10
12	ELC	1	0.3	0	2.67	10				
12	SRR	2						3	10	10
13	ELC	1	0.3	0	2.67	10				
13	SRR	2						3	10	10
14	ELC	1	0.45	0	2.67	10				
14	SRR	2						3	10	5
15	ELC	1	0.45	0	2.67	10				
15	SRR	2						3	10	5
16	ELC	1	0.45	0	2.67	10				
16	SRR	2						3	10	5
17a	ELC	1	0.35	0	10	10				
17a	SRR	4						3	10	5
17b	ELC	1	0.35	0	10	10				
17b	SRR	6						3	10	10
18a	ELC	1	0.35	0	10	10				
18a	SRR	4						3	10	5
18b	ELC	1	0.35	0	10	10				
18b	SRR	6						3	10	10
19a	ELC	2	0.35	0	10	10				
19a	SRR	7						3	10	5
19b	ELC	1	0.35	0	10	10				
19b	ELC	1	0.55	0	10	10				
19b	SRR	3						3	10	5
19b	SRR	4						3	2.2	5
20a	ELC	2	0.35	0	10	10				
20a	SRR	7						3	10	5
20b	ELC	1	0.35	0	10	10				
20b	ELC	1	0.55	0	10	10				
20b	SRR	3						3	10	5
20b	SRR	4						3	2.2	5
22a	ELC	1	0.25	3	10	5				
22b	ELC	1	0.25	3	10	5				
22b	SRR	9						3	10	5
22c	SRR	9						3	10	5
23a	ELC	1	0.25	3	10	5				
23b	ELC	1	0.25	3	10	5				
23b	SRR	9						3	10	5
23c	SRR	9						3	10	5
24a	ELC	1	0.55	0	10	10				
24b	ELC	1	0.45	0	10	10				
24c	ELC	1	0.35	0	10	10				
24d	ELC	1	0.25	0	10	10				
25a	ELC	1	0.25	1	10	10				
25b	ELC	1	0.25	2	10	10				
25c	ELC	1	0.25	3	10	10				
26a	SRR	1						3	10	5
26b	SRR	1						3	2.2	5
26c	SRR	1						3	1.5	5
26d	SRR	1						2	1.5	5
26e	SRR	1						1	1.5	5